



Hirshfeld surface analysis, enrichment ratio, energy frameworks and third-order nonlinear optical studies of a hydrazone derivative for optical limiting applications



Laxminarayana Kamath^a, Anthoni Praveen Menezes^{b,*}, Raghavendra Bairy^c,
Shashi Kumar Kumara swamy^a, A. Jayarama^a

^a Department of Physics, Alva's Institute of Engineering & Technology, Shobhavana Campus, Mijar, Moodabidri, 574225, India

^b Department of Physics, Mangalore Institute of Technology & Engineering (MITE), Moodabidri, 574 225 India

^c Department of Physics, N.M.A.M. Institute of Technology, Nitte, Udipi, 574110, India

ARTICLE INFO

Article history:

Received 21 October 2020

Revised 19 May 2021

Accepted 30 June 2021

Available online 4 July 2021

Keywords:

Hydrazone

Hirshfeld analysis

Enrichment ratio

Interaction energy

nonlinear refraction

Optical Limiting

ABSTRACT

Organic materials with good third-order nonlinear optical (NLO) properties are used in optoelectronics for protecting human eyes and sensors from high intensity laser light. In this regard, herein we report the synthesis, structural analysis, and third-order NLO properties of an organic molecule *N'*-(*E*)-(4-fluorophenyl)methylidene]biphenyl-4-carbohydrazone (FMBC) containing hydrazone moiety. The formation of the synthesized molecule is confirmed by identifying the functional groups through FTIR spectral analysis. The material possesses good thermal stability before the melting point of 242.5 °C and transparent in the entire visible region of the EM spectrum. The photoluminescence study revealed the blue light-emitting property of FMBC. The crystal structure is stabilized by N-H...O, C-H...O, and C-H...F hydrogen bond interactions. The interconnects in the crystal packing were envisioned quantitatively using Hirshfeld surfaces (HS) by 2D fingerprint plots. The main contribution to the HS comes mainly from C-H, H-H, and O-H interconnects which cover about 80 % of the total HS surface. The enrichment ratios show that the favorable contacts accountable for the crystal packing are C...H, N...H, O...H, and F...H. The breakdown of the interaction energies obtained for various molecular pairs shows the nature and strength of the interactions. The calculation of 3D energy frameworks suggests that contacts formed in the structure are largely due to the dispersion force followed by the electrostatic potential. Third-order NLO coefficients were extracted under the continuous wave (CW) regime using *z*-scan technique. The material is an excellent optical limiter with a threshold value of 3.42 kJ/cm².

© 2021 Elsevier B.V. All rights reserved.

1. Introduction

The ultimate goal of crystal engineering is to synthesize crystalline materials for application on nonlinear optics (NLO) and optoelectronic systems with specific physicochemical properties. Materials possessing excellent third-order nonlinear optical properties could be used in optical switching, optical signal processing optical limiting, and such other applications [1,2,3]. Materials with substantial nonlinear refractive indices are appropriate for light transmission based devices whereas those with large nonlinear absorption are best suited for optical switching and sensor protection applications [4]. Among the various types of materials investigated for NLO properties, organic materials are in focus due

to their versatile properties which include high optical nonlinear and electro-optic coefficients, fast response, flexibility in modifying the structure, ease of fabrication, and incorporation in devices for various photonic applications [5,6,7]. Recently, the organic material *N*-acyl hydrazone attracted extensive interest due to its ease of synthesis, presence of various isomers, and various potent properties. The hydrazone moiety, -C(=O)-NH-N=CH- in an organic molecule, leads to the nucleophilic and electrophilic effect in the molecule [8,9]. Attachment of the electron-donating/ withdrawing groups across this bridge results in a push-pull structure with improved molecular polarizability and optical nonlinearity.

Schiff bases are an important class of organic materials with exciting third-order NLO properties. The aromatic rings substituted on either side of the π -electron bridge (-C=N-) enhances the delocalization of the π -conjugated electron in these type of materials. The magnitude of the NLO coefficients largely depends on the length of conjugation, molecular conformations, and electron

* Corresponding author.

E-mail address: mapraveen.80@gmail.com (A.P. Menezes).

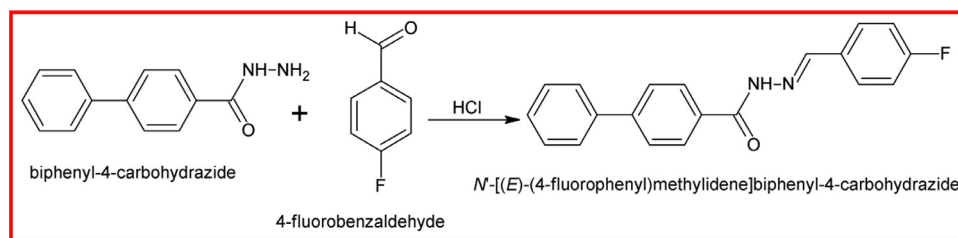


Fig. 1. Scheme for the synthesis of FMBC.

donor/acceptor groups. The azomethine group/ hydrazone core being an electron donor, the substitution of a more functional group on the hydrazone moiety further enhances the number of donor sites and thus the molecular nonlinearity [10]. The integration of various substituents with appropriate donor/acceptor strength into the aromatic rings also boosts the molecular binding affinities via intermolecular interactions and π -electron delocalization and as a consequence the optical nonlinear behavior increases. Keeping these aspects in mind, we synthesized a Schiff base, *N'*-[(*E*)-(4-fluoro Phenyl)methylidene]biphenyl-4-carbohydrazide (FMBC) having large conjugation length [11]. Since the material crystallizes in centrosymmetric $C2/c$ space group second-order nonlinearity hard to observe. Therefore, the third-order nonlinear properties such as nonlinear absorption (β), nonlinear refractive index (n_2), and the nonlinear optical susceptibility ($\chi^{(3)}$) were extracted by performing a single beam z-scan experiment. Herein, we report the synthesis, thermal, photoluminescence, linear, and nonlinear optical studies of FMBC. The structural details obtained from single-crystal X-ray diffraction is also provided for ready reference. The contribution of intermolecular interactions to crystal packing and nonlinear behavior is analyzed through the Hirshfeld surface analysis (HS), interaction energy calculations, enrichment ratios, 3D energy framework, and 2D fingerprint plots.

2. Materials and methods

2.1. Synthesis

The title compound, *N'*-[(*E*)-(4-fluorophenyl) methylidene] biphenyl-4-carbohydrazide (FMBC) was synthesized using 4-fluorobenzaldehyde and biphenyl-4-carbohydrazide as the starting materials. The chemicals with 99.99% purity were procured from Sigma Aldrich Inc. and were used without further purification. Equimolar quantities of the precursors were dissolved separately in 30 ml of ethanol. Two drops of Conc. HCl acid was added, and the mixture was refluxed for 3 h. The mixture is then allowed to cool, the solid precipitate formed was washed with water and dried. Shown in Fig. 1 is the synthesis process schematic. The composition of the product - Found (calculated): C: 75.40 % (75.46%); H: 4.78 % (4.75 %); N: 8.73% (8.80%). The single crystals were grown by slow evaporation of the solvent method at ambient temperature choosing DMF as the solvent.

2.2. Characterization and computational techniques

The formation of the compound was confirmed by identifying the functional groups present in FMBC through FT-IR spectroscopy. The spectrum is recorded using the pellet technique wherein the sample is mixed with KBr powder and a disk is formed. The spectrum is recorded in the wavenumber range 4000-400 cm^{-1} using a SHIMADZU-8400S FT-IR spectrometer with a spectral resolution of 0.1 cm^{-1} . To explore the temperature range over which the material can be used, the melting point and the decomposition temperature was determined by thermogravimetric (TG) and differen-

tial thermal (DT) analysis of FMBC. The sample was scanned in the temperature range 30°C - 600 °C at the heating rate of 10 °C/min in the nitrogen atmosphere using SDT Q600 V20.9 Build 20 thermal analyzer. The linear optical absorption/transmission spectrum was recorded in the wavelength region 200 nm to 900 nm using a UV-1601PC UV-Visible spectrophotometer. The specimen is dissolved in DMF (0.01M) and taken in a 1 mm thick quartz cuvette and exposed to the radiation. The photoluminescence (PL) study was carried out on FMBC using the FluoroMax-4CP spectrometer. The sample was dissolved in DMF and the experiment was conducted in the range 400 nm to 800 nm at room temperature by exciting the sample with a radiation of wavelength 380 nm. The signal was detected using the R928P photomultiplier tube with a resolution of 0.2 nm. The interatomic contacts present in the solid structure which contribute to the stabilization of bulk structure were analyzed by Crystal Explorer 17.5. The Hirshfeld surfaces (HSs), 2D fingerprint plots (FPs) interaction energies and energy 3D-frame works of FMBC were obtained using the crystallographic information file (.cif) as the input [12]. The third-order nonlinear optical parameters were evaluated by performing the classical Z scan experiment [13]. A continuous-wave laser beam of wavelength 532 nm with 200 mW output power from a diode-pumped solid-state laser source was focused onto a 1 mm thick cuvette containing the 0.01M solution of FMBC prepared in DMF. The laser beam of peak input intensity of $I_0 = 8.48 \times 10^7 \text{W/m}^2$ was focused using a lens of focal length 28.6 cm. The thin sample approximation is applicable in this case as the sample thickness is much smaller than the equivalent Rayleigh length z_0 (8.86 mm). The beam waist at the focus was estimated to be equal to 38.75 microns. The sample is moved using a computer-controlled translational stage and far-field light intensity variation is noted with and without aperture in front of the detector using Laser Probe Rj-7620 Energy Meter with pyroelectric detectors.

3. Results and discussions

The recorded IR spectrum of the title compound is displayed in Fig. 2. The spectrum shows a broad absorption band at 3403 cm^{-1} corresponding to the N-H vibration and the weak band at 2937 cm^{-1} represents the presence of aromatic C-H stretching vibration. The strong band at 1645 cm^{-1} indicates the -C=O- group while the C-F stretching is confirmed by the weak band observed at 1089 cm^{-1} . The medium intensity peak at 1395 cm^{-1} confirms the C-N stretching vibrations. Thus, the analysis of the FT-IR spectrum confirms the formation of the title compound, FMBC.

Fig. 3 depicts 1D ^1H (Hydrogen) NMR spectra of the title compound - FMBC. The ^1H - Chemical shifts are referenced to Dimethylsulfoxide (DMSO- d_6 peak 2.49 ppm, solvent reference) and were analyzed in accordance with standard ^1H Chemical shift database. The occurrence of crowded aromatic hydrogen signals in the ^1H chemical shift range of 7 - 8 ppm indicates signal arising from 13-methine protons (C^{-1}H) from the aromatic ring of dibenzyl moiety. The upfield shifted aliphatic methine (C^{-1}H) is found at 3.3 ppm which arises from the carbon linking dibenzyl and fluoreben-

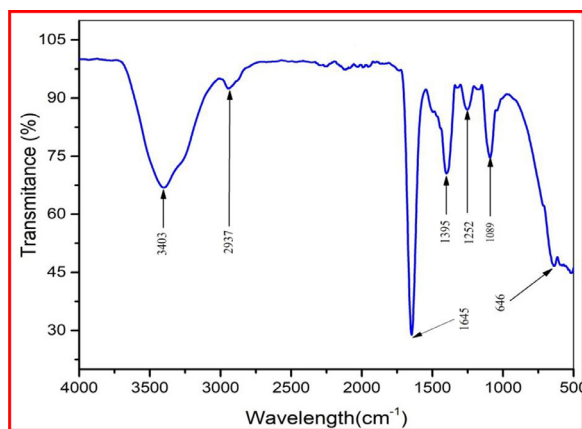


Fig. 2. FT-IR spectrum of FMBC.

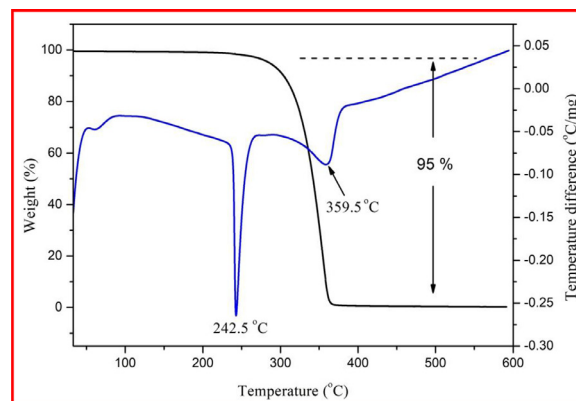


Fig. 4. TG/DTA plot of FMBC.

zyl moiety. Further extreme downfield shifted amide ($N-H$) signal at 11.94 ppm arising from the hydrogen attached to linking nitrogen, double validates the formation of the FMBC compound.

The thermal stability of the material for high-temperature applications is investigated by Thermogravimetric and differential thermal analysis. The recorded thermograms are shown in Fig. 4. The sharp endothermic peak observed at 242.5 °C is the temperature at which the material undergoes melting. The absence of weight loss at the melting is evident from the TGA curve. Moreover, the material starts losing its weight at about 275 °C. The material undergoes decomposition at 359.5 °C. The major weight loss of about 95 % occurs in the temperature range of 310 °C – 380 °C. Up to the melting point no phase transitions were found and thus FMBC forms a useful candidate in high-temperature applications.

Linear optical absorption studies were carried out to explore the transmission window of the crystal for optical applications. The UV-VIS absorption and transmission spectra of FMBC are reported in Fig. 5 which reveals that the crystal has a broad transmission window covering the entire visible region of the EM spectrum. The minimum absorption in the visible region of the EM spectrum enables the material to be used for NLO applications because the larger the absorption, the greater will be the loss of conversion efficiency in the region of interest. Using the linear absorption data, the optical bandgap of the material is obtained by plotting

the Tauc's plot [14]. The curve of $(\alpha h\nu)^2$ against photon energy is shown in Fig. 6. In this case, the absorption coefficient α is determined using the relation, $\alpha = 2.303(A/t)$, A being the absorbance and t the sample thickness. The linear nature of the curve can be considered as evidence for the indirect transition taking place in the material [15]. The optical band gap is obtained by extrapolating the linear portion of the curve to the energy axis as shown in Fig. 6 and the value is found to be 3.44 eV. The large transmittance in the visible region is the consequence of this wider bandgap.

The emission and excitation properties of the title crystal were examined by Photoluminescence (PL) spectral studies. This is a non-destructive technique of identifying defects by the mechanism of color center creation [16]. The recorded spectrum of FMBC shown in Fig. 7 shows a broad high-intensity emission peak at centered on 431 nm. The broad emission peak in the PL spectrum is ascribed to the strong intra-molecular interaction present within FMBC crystal. The broad emission peak confirms the light emission in the blue region and can be used as blue light-emitting material in optoelectronics such as for blue LEDs. Furthermore, the single color emission peak observed in the explored region suggests the good crystallinity and structural perfection of the grown FMBC crystals [17].

The single-crystal X-ray diffraction study of FMBC, reported by G. Dutkiewicz et al [11] showed that FMBC crystallizes in the monoclinic crystal system with the centrosymmetric $C2/c$ space group. The unit cell parameters are, $a = 37.163(5)$ Å. $b = 10.692(2)$ Å,

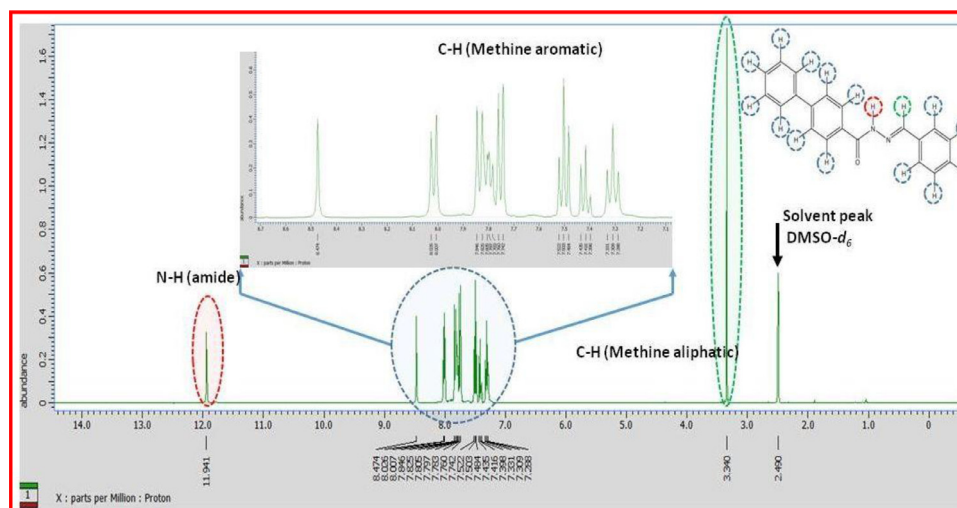


Fig. 3. 1H (Hydrogen) NMR spectrum of FMBC.

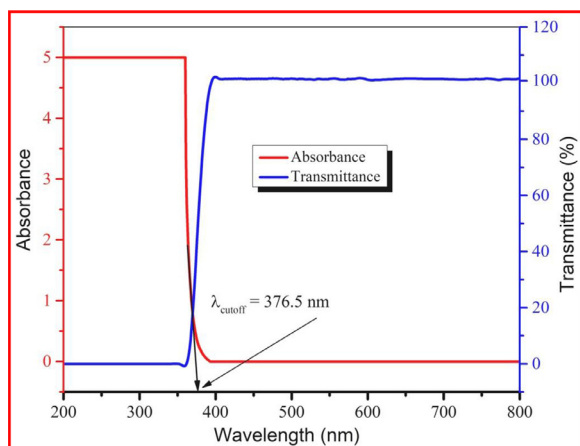


Fig. 5. UV-VIS spectrum of FMBC.

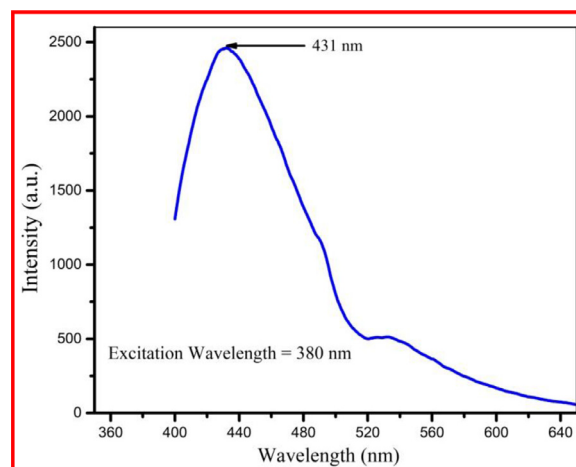


Fig. 7. PL spectrum of FMBC.

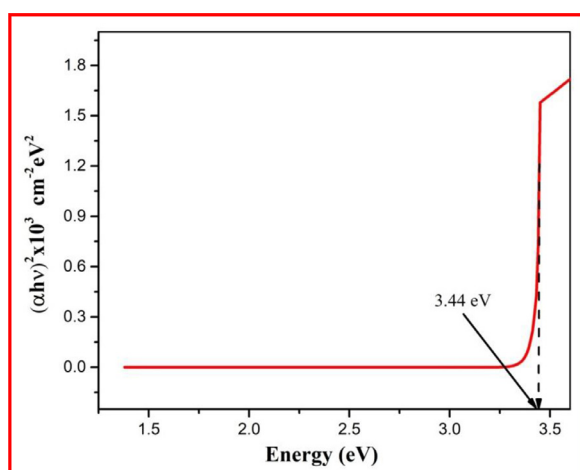


Fig. 6. Tauc Plot of FMBC.

$c = 8.98(2) \text{ \AA}$, $\beta = 101.18(2)^\circ$. The structure of the FMBC molecule with 50 % probability ellipsoids is shown in Fig. 8. A detailed description of the structure can be found in the literature [11]. The structure is stabilized by N-H...O, C-H...O, and C-H...F interactions as shown in Fig. 9. The N-H...O hydrogen bond interactions help the molecules to pack into the infinite chains along crystallographic c direction as shown in Fig. 9 and Fig. 10. Also, there exists a highly directional C-H...F interaction which helps the molecules to form a stable crystal structure. The atoms of the C=N-N-C=O bridge namely C8, N8, N9, C10, and O11 are coplanar [11], and this plane makes an angle of 13° with the phenylene ring and makes an angle of 22.05° with the mean plane through the biphenyl rings of the benzoyl arm. The fragments of the biphenyl rings are twisted by an amount of 23.14° . The terminal benzene rings lie

almost on a single plane as indicated by the dihedral angle of 2.83° between their mean planes. Thus, the FMBC molecule as a whole has a nearly planar structure.

The analysis of calculated Hirshfeld surfaces is now an invaluable tool, as it provides further insight into the various intermolecular interactions that influence the packing of molecules in crystals. Crystal Explorer 17.5 computer program was used to generate the Hirshfeld Surface (HS) and 2D fingerprint plots of FMBC [18]. The intermolecular interactions with the adjacent molecules are evaluated by the colour shading range of -0.542 (red region) to 1.524 (blue region) in terms of distances ' d_e ' (the distance between the surface and the nearest nucleus outside the surface) and ' d_i ' (distance between the surface and the nearest nucleus inside the surface). These distances allow us to analyze the intermolecular interactions through the mapping of d_{norm} . The STO-3G (Slater-type orbitals simulated by 3 Gaussians) basis set at the Hartree-Fock theory wave function calculations were used to obtain electrostatic potentials mapped over the Hirshfeld surface over the range of -0.030 \AA (red) to 0.020 \AA (blue). To calculate the electrostatic potential, the experimental geometry obtained from the single-crystal X-ray diffraction study was used with TONTO integrated into Crystal Explorer program [19]. These plots help in understanding the crystal packing by visualizing the various intermolecular interactions. The short but strong interatomic contacts appear as red spots on the d_{norm} surface (Fig. 11a) while other weak interactions with positive d_{norm} value are represented in blue. The surfaces mapped over shape index and curvedness properties shown in Fig. 11b and Fig. 11c helps to identify the different packing modes and the interconnections between nearby molecules. Through the shape index map of the HS, one can visualize the existence of π - π stacking interactions. From Fig. 11(b), it is clear that there are no such interactions present in FMBC which is evident from the absence of adjacent red and blue triangular regions. This is further confirmed by

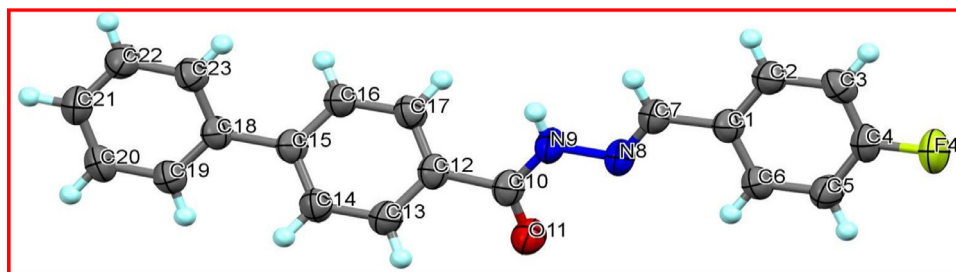


Fig. 8. Molecular structure of FMBC shown with 50 % probability ellipsoids.

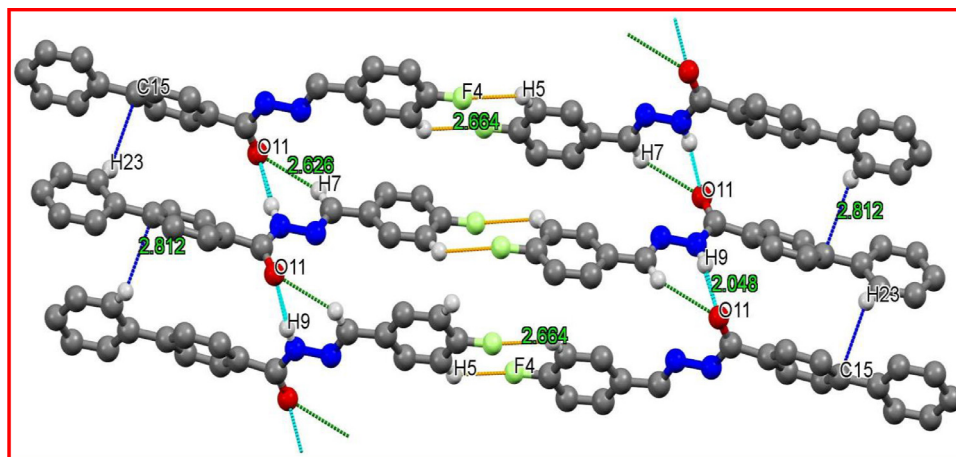


Fig. 9. Packing diagram of FMBC showing hydrogen bond interactions.

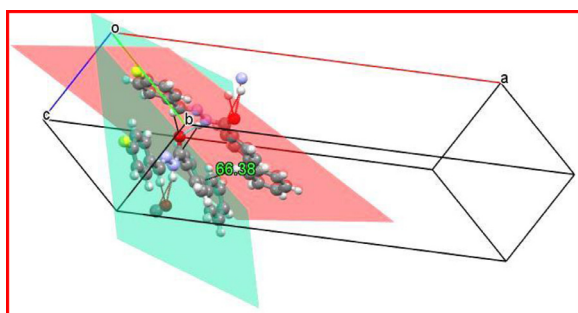


Fig. 10. Packing diagram of FMBC showing orientation of dipoles along the *c*-direction.

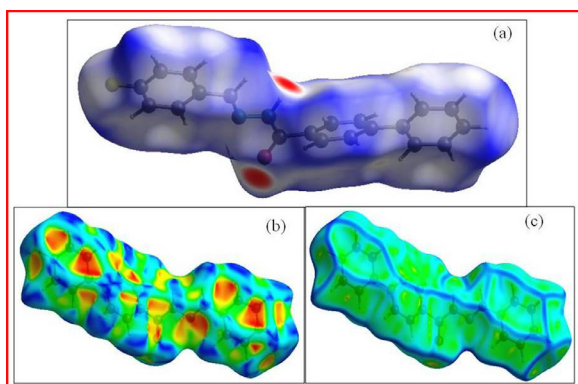


Fig. 11. Hirshfeld surfaces mapped over (a) d_{norm} , (b) shape index, and (c) curvedness.

the absence of flat regions and the dark blue edges on the curvedness map. The concave-shaped regions in bright red (red hollow with shape index <1) indicate the acceptor atoms while convex regions in blue color (blue bumps-shape with shape index >1) appear around the donor atoms on the HS mapped with shape index [20]. Fig 12(a) is the d_{norm} surface showing N-H \cdots O interaction with a dark red spot on N-H atom and the oxygen atom due to the presence of strong H₉ \cdots O₁₁ hydrogen bond in the title compound. The electrostatic potential surface displayed in Fig. 12 (b) and Fig. 12(c) further establishes the N-H \cdots O interaction where the atoms involved in strong hydrogen bonds are seen as dark-blue and dark-red regions. The red regions in these plots represent the negative electrostatic potential corresponding to the acceptors and

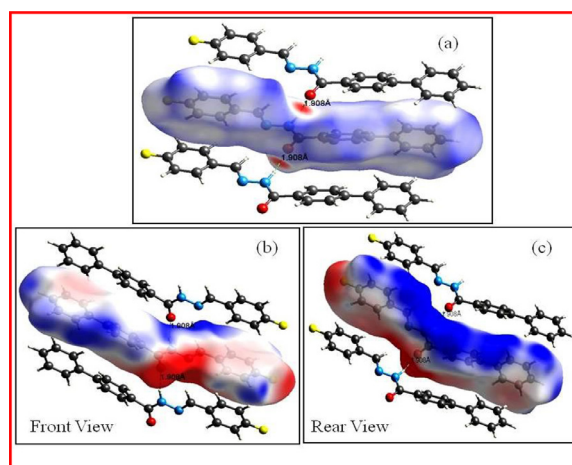


Fig. 12. Hirshfeld surfaces mapped over (a) d_{norm} and (b, c) electrostatic potential of FMBC showing N-H \cdots O hydrogen bond interactions as dashed lines.

the donors with positive electrostatic potential are shown as blue regions.

The 2D fingerprint .plot is a useful method to represent the complex information incorporated in a crystal. It provides a visual summary of the frequency of the different combinations of d_e and d_i values across the Hirshfeld surface of a molecule. A fingerprint plot, which is divided into certain specific interatomic contact, provides information about that specific intermolecular interaction. The fraction of the various intermolecular interactions that contribute to the overall HS of FMBC is shown in Fig. 13 and Fig. 14 along with the portion of the HS covered by each type while the relative contributions are summarized in Fig. 15. The main contribution to the surface arises from C \cdots H and H \cdots H interactions covering 37.9 % and 32.5 % of the HS respectively. The reciprocal contacts on H \cdots O, H \cdots F intermolecular interactions appeared as two sharp needles with $d_e + d_i \cong 2.28$ Å for H \cdots O and with $d_e + d_i \cong 2.82$ Å for H \cdots F interaction. The H \cdots C interaction appeared as the symmetrical wing, $d_e + d_i \cong 3.28$ Å with significant contribution to the packing of the crystal. The other major contributor for crystal packing is H \cdots H interatomic contact, appeared as a diffused needle with $d_e + d_i \cong 2.44$ Å.

Surface contact data derived from the HS analysis are used to derive enrichment ratios (ER) that enable to analyze the tendency of chemical species to interact in pairs in forming crystal packaging and are tabulated in Table 1 [21]. The ER values for C \cdots H, N \cdots H,

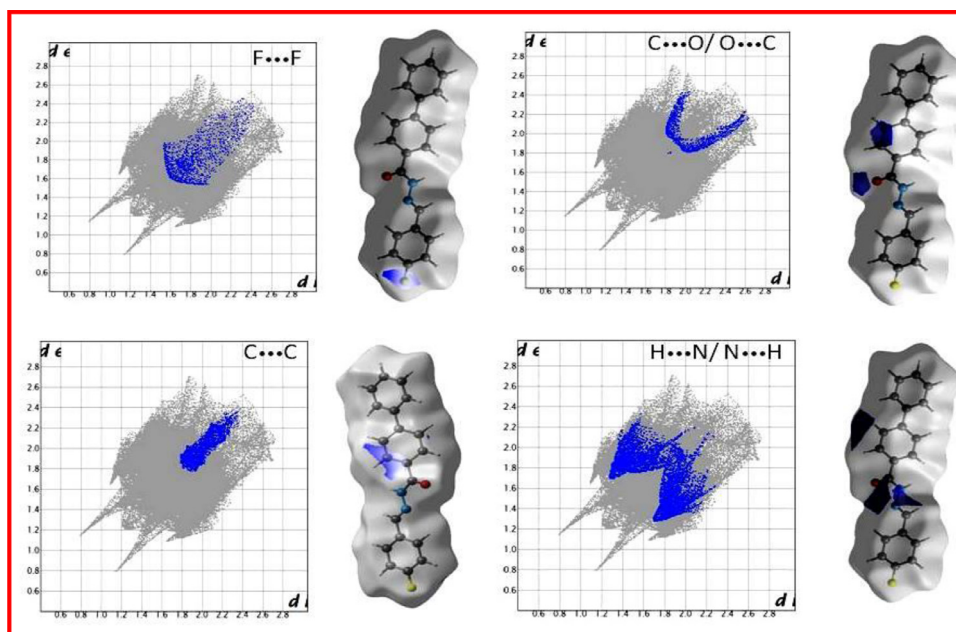


Fig. 13. 2D fingerprint plots for FMBC delineated into F...F, C...O, C...C, and H...N contacts.

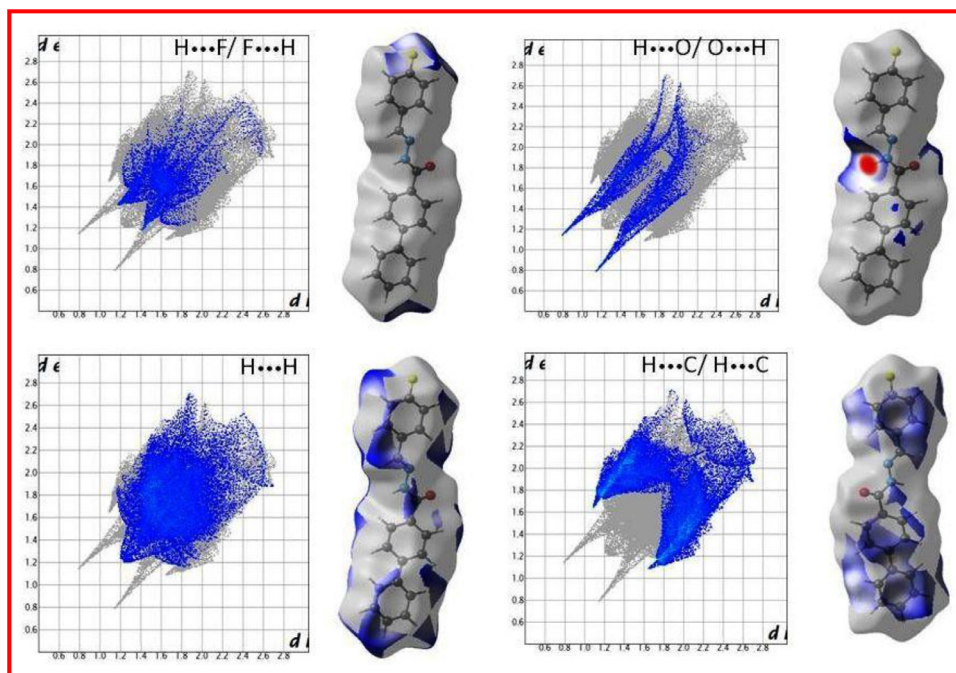


Fig. 14. 2D fingerprint plots for FMBC delineated into H...F, H...O, H...H, and C...H intercontacts.

O...H, and F...H are greater than unity indicating that these pairs have a larger propensity to form interconnects in the crystal structure whereas the pairs with random contacts fewer than 0.9 % are ignored. The C...C and O...C inter-contacts have ER values 0.62 and 0.61 respectively and are less likely to form contacts in the crystal. The H...H self-contact is also not favoured with an ER value of 0.74.

Furthermore, the intermolecular interaction energies between the molecular pairs in FMBC were calculated using the Crystal Explorer 17.5 software. These energy values were further used to visualize and analyze the predominant interactions in the molecular crystals packing as 3D energy frameworks [22,23]. A cluster of molecules was built around a selected reference molecule within a radius of 3.8 Å and the interaction energy was calculated by gener-

ating the wave function using the most accurate B3LYP/6-31G(d,p) level of theory. By applying crystallographic symmetry operations, the encircling molecules in the shell around the central molecule were obtained. Within the defined radius (shell) there are a total of ten molecules that are involved in the dimer formation. These molecular energy interaction pairs enable the total energy to be divided into different components such as electrostatic (E_{ele}), dispersion (E_{dis}), repulsion (E_{rep}), and polarization (E_{pol}). Mackenzie's method was adopted to partition the total energy benchmark with 1.057, 0.871, 0.618, and 0.740 as the scale factors, for electrostatic, dispersion, repulsion, and polarization respectively [22]. The calculated interaction energies between the dimers within the default shell are given in Table 2. Fig. 16 is the visualization of the interac-

Table 1

Hirshfeld surface contacts, the derived random contacts, and ER values for the FMBC by atom type. The data values obtained from Crystal Explorer 17.5 program are written in italics at the top of the table. The table does not include the ER for random contacts less than 0.9 % as they do not mean.

Atoms	H	C	N	O	F
H	32.5				
C	37.9	2.5			
N	6.8	-	-		
O	9.2	1.3	-	-	
F	8.7	-	-	-	1.0
Surface %	61.27	24.57	3.58		5.55
H	43.77				
C	26.51	4.01			
N	4.23	1.28	0.10		
O	7.00	2.12	0.34	0.28	
F	7.05	2.13	0.34	0.56	0.28
H	0.74				
C	1.43	0.62			
N	1.61	-	/		
O	1.31	0.61	/	/	
F	1.23	-	/	/	/

Table 2

Interaction Energies (kJ/mol) with symmetry operations (symop) for FMBC. R is the distance between molecular centroids (mean atomic position) in Å. Total energies are the sum of the four energy components, scaled appropriately. The energy model used CE-B3LYP ... B3LYP/6-31G(d,p) electron densities with K_ele (1.057), K_pol (0.740), K_disp (0.871) and K_rep (0.618). Refer to Fig. 14 for color codes.

N	Symop	R	E_ele	E_pol	E_dis	E_rep	E_tot
1	-x, -y, -z	17.99	-3.9	-0.4	-7.5	5.2	-7.8
0	-x+1/2, y+1/2, -z+1/2	6.21	-14.7	-3.1	-33.5	16.8	-36.6
1	x+1/2, y+1/2, z	19.52	-0.7	-0.3	-5.7	2.9	-4.1
0	-x+1/2, -y+1/2, -z	5.88	-3.4	-2.7	-35.7	18.1	-25.5
1	-x, y, -z+1/2	17.64	-1.2	-0.4	-8.2	2.6	-7.1
1	x, -y, z+1/2	4.07	-53.7	-13.0	-72.3	82.5	-78.4
0	-x+1/2, y+1/2, -z+1/2	7.34	-3.8	-1.1	-16.7	8.9	-13.9
1	-x+1/2, -y+1/2, -z	5.05	-3.8	-2.2	-54.1	24.4	-37.7
0	-x, -y, -z	19.60	0.5	-0.2	-4.8	1.5	-2.8
0	-x, y, -z+1/2	18.87	-0.6	-0.2	-6.9	2.2	-5.4
Total Energy			-85.3	-23.6	-245.4	165.1	-219.3

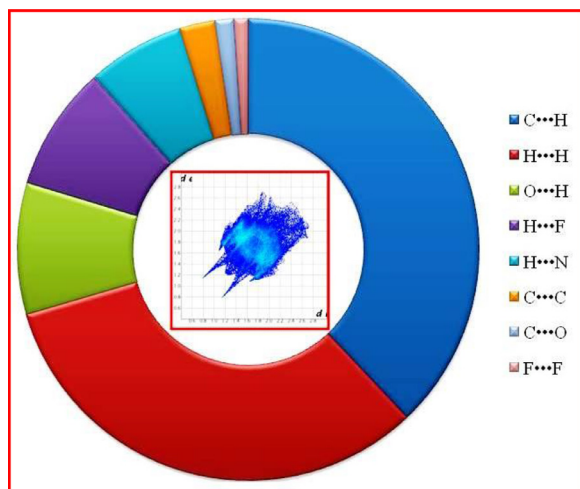


Fig. 15. The relative contribution of intermolecular contacts in FMBC to the Hirshfeld surface. Inset is the full 2D fingerprint plot.

tion energies via the color codes. The total interaction energies delineated into electrostatic, polarization, dispersion, and exchange-repulsion respectively are -85.3 kJ/mol, -23.6 kJ/mol, -245.4 kJ/mol, and 165.1 kJ/mol. The total interaction energy is found to be -219.3 kJ/mol. These energy values show that the overall stability of the structure is mainly due to the dispersion force followed by the electrostatic potential force.

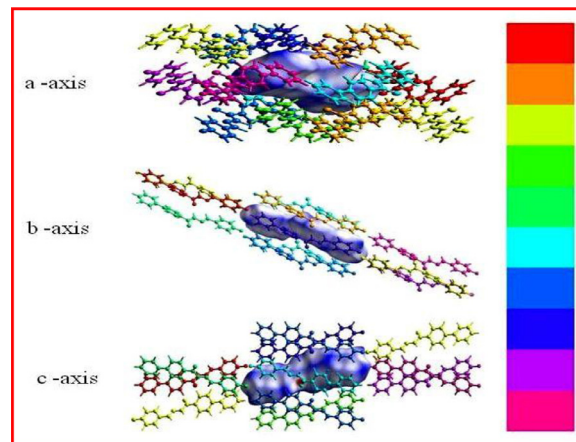


Fig. 16. Color coding of the adjacent molecules concerning the central molecule (shown with HS) viewed along a,b,c axes.

An extended characteristic established by the calculation of interaction energies is the simulated 3D energy framework. These energy frameworks enable one to have a better understanding of the topology of the overall interaction energies among various parts of the crystal. The framework is obtained by generating a cluster of molecules within a $1 \times 1 \times 1$ unit cell. The generated frameworks are presented in Fig. 17. The relative strengths of molecular packing interaction energy in all directions are indicated by the cylindrical shapes where the radii of the rods are pro-

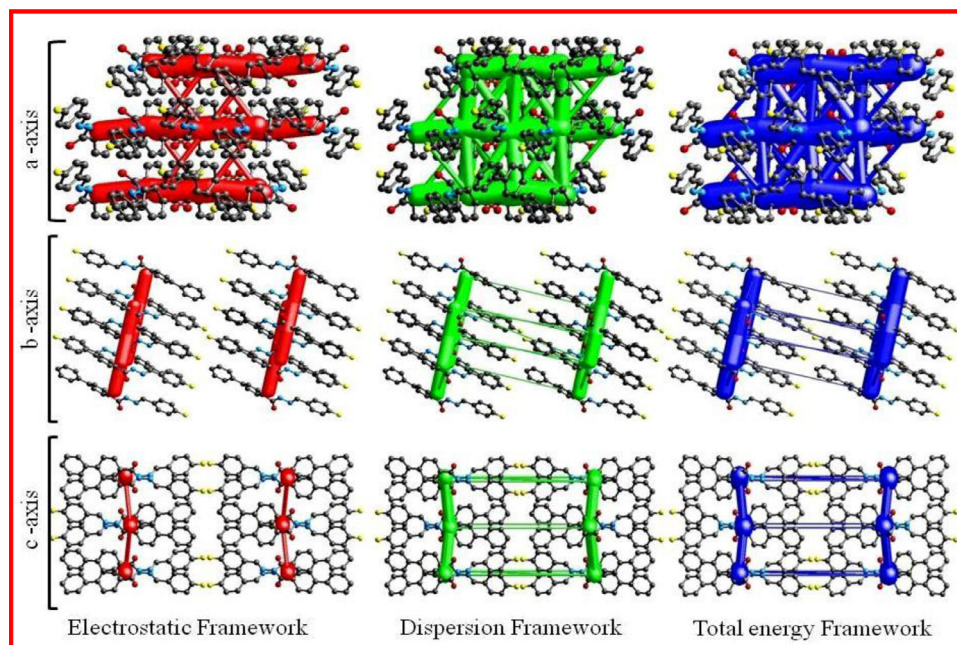


Fig. 17. Energy framework diagrams for E_{ele} (red tubes), E_{dis} (green tubes), E_{tot} (blue tubes) for a cluster of molecules within $1 \times 1 \times 1$ unit cell of FMBC viewed down the a,b,c-axes.

portional to the magnitude of the interaction energy in a different direction. The energy frameworks for electrostatic, dispersion and total energy components are shown in red, green, and blue colored tubes. All the frameworks were adjusted to the same cylinder scale factor of 150. Weak and insignificant contacts less than the 5 kJ / mol threshold were not included in the calculation.

Third-order NLO parameters (n_2 and β) were estimated by the well known single beam Z scan experimental procedure. The nonlinear refractive index is determined by measuring the intensity of the light transmitted by the sample as it moves along the focal length of the beam. In this case, the light intensity is detected after passing it through an aperture (close aperture mode). The beam experiences a nonlinear phase shift $\Delta\theta$ as it passes through the sample which leads to the variation in the amount of light falling on the detector. The shape of the curve and thus the relative position of the peak and valley on the Z-axis depend on the nonlinear phase shift [24]. Fig. 18(a) confirms that the normalized transmittance exhibits a transmission maximum (peak) before the focus and a transmission minimum (valley) after the focus. This peak-valley configuration is a signature of self-defocusing effect in FMBC (negative nonlinear refractive index). Further, the curve is asymmetric and thus it can be inferred that when the sample is scanned with a CW laser beam, the laser beam gets distorted due to the spatial thermal variation. Hence the nonlinear refraction observed in FMBC is of thermal origin. The magnitude and sign of n_2 can be obtained by fitting the experimental closed aperture normalized transmittance with the theoretical equation,

$$T(z) = \left[1 - \frac{(4x\Delta\theta)}{(x^2 + 1)(x^2 + 9)} \right] \quad (1)$$

Where $x = z/z_0$ and $\Delta\theta$ is the nonlinear phase shift. The magnitude of n_2 can be found from the relation, $\Delta\theta = kn_2I_0L_{eff}$. In this equation, k is the wave vector ($k = 2\pi/\lambda$), $L_{eff} = [1 - e^{-\alpha L}]/\alpha$, is the effective thickness of the sample, and α is the linear absorption coefficient.

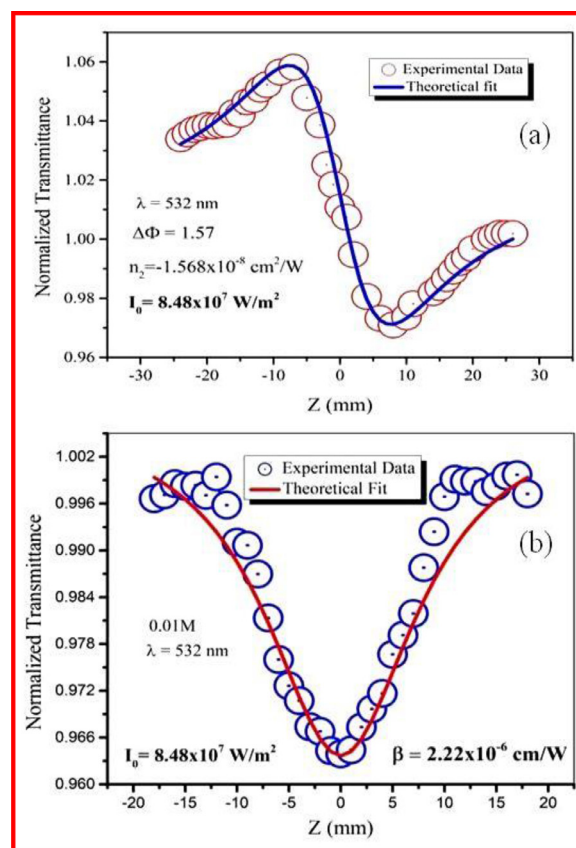


Fig. 18. (a) Closed aperture curve, (b) open aperture curve of FMBC.

The experimental open aperture data were fitted with the equation (2) to extract the β value [13] [25].

$$T(z) = 1 - \frac{I_0 L_{eff} \beta}{2\sqrt{2}} \left[\frac{1}{1 + x^2} \right] \quad (2)$$

Table 3
Third-order nonlinear optical parameters of FMBC.

λ	n_2	β	$Re \chi^3$	$Im \chi^3$	χ^3	γ_h
(m)	(cm^2/W) (cm/W) (esu) (esu) (esu) (esu)					
$\times 10^{-9}$	$\times 10^{-8}$ $\times 10^{-6}$ $\times 10^{-7}$ $\times 10^{-7}$ $\times 10^{-7}$ $\times 10^{-26}$					
532	-1.568 2.22 6.724 3.896 6.72 4.877					

Table 4
The absorption cross-sections and optical limiting threshold value of FMBC.

σ_2	σ_2^1	σ_{ex}	σ_g	OL Threshold
(cm^4/W) (cm^4S) (cm^2) (cm^2) (J/cm^2)				
$\times 10^{-25}$ $\times 10^{-43}$ $\times 10^{-20}$ $\times 10^{-23}$ $\times 10^3$				
3.69		1.38	1.92 6.1 3.42	

The experimental and theoretically fitted open aperture curves are shown in Fig. 18(b). It is evident from the shape of the plot that the title compound exhibits two-photon absorption with reverse saturation (Table 4). The positive NLA coefficient of FMBC is confirmed from the fact that the light intensity is least at the focus ($Z = 0$) and increases symmetrically on either side of it [26]. The estimated values of n_2 and β were used to determine the molecular second-order hyperpolarizability γ_h which is the indication of induced nonlinear molecular polarization. The quantity γ_h is related to the macroscopic third-order nonlinear optical susceptibility $\chi^{(3)}$ through the equation,

$$\gamma_h = \frac{\chi^{(3)}}{N_A C ((n_0^2 + 2)/3)^4 \times 10^{-3}} \quad (3)$$

Here, C is the concentration (mole/cm³), N_A is the Avogadro number, and n_0 is the linear refractive index. $\chi^{(3)}$ is obtained using the relations [27],

$$|\chi^{(3)}| = \left[(Re \chi^{(3)})^2 + (Im \chi^{(3)})^2 \right]^{1/2} \quad (4)$$

$$Re \chi^{(3)} (e.s.u) = \frac{(\epsilon_0 c^2 n_0^2 n_2)}{\pi} \quad (5)$$

$$Im \chi^{(3)} (e.s.u) = \frac{(\epsilon_0 c^2 \beta n_0 \lambda)}{\pi} \quad (6)$$

The magnitudes of the various third-order nonlinear optical parameters thus obtained are presented in Table 3 and Table 4. The values of molecular two-photon absorption coefficient (σ_2), molecular two-photon absorption coefficient (σ_2^1), excited-state absorption coefficient (σ_{ex}), and ground-state absorption coefficient (σ_g) were estimated by using the equations presented in the literature [26]. The computed values of n_2 , β , χ^3 , and γ_h are compared with those of some of the well characterized organic materials under the CW regime and are tabulated in Table 5.

The observed good third-order NLO coefficients of FMBC under investigation can be understood from the molecular structure and stacking of molecules in the crystal structure. The molecule consists of a hydrazone group (-C(=O)-NH-N=CH-) as can be seen in Fig. 8. The benzene ring with fluoro group attached to its para position (phenylene group) at one end of this chain acts as an electron donor moiety. The carbonyl group (-C=O-) is an electron-withdrawing group that attracts the charges from the biphenyl group at the other end of the hydrazone chain. Thus, FMBC is a donor- π -acceptor- π -donor (D- π -A- π -D) type structure where charges flow ends of the molecule towards the center [29]. Since a strong electron donor is placed at the para position of the benzene ring, there is an effective transfer of charge from that ends to the center of the molecule resulting in the delocalization of charges

[34,35]. This kind of charge transfer increases the π -electron density through improved conjugation, which in turn contributes to the improvement in the NLO property of a material. Besides, the hydrogen bonds, optimized alignment of the molecular dipoles in the bulk, molecular planarity play an important role in the optical nonlinearity of the material. From the X-ray diffraction studies and the HS analysis, we found that the crystal structure of FMBC is stabilized by the strong N-H \cdots O and C-H \cdots F hydrogen bond interaction. The benzoyl and the phenylene moieties are interconnected via a planar C=N-N-C=O chain and this planar backbone enables an effective flow of charge from the ends of the molecule towards the center [11]. None the less, these hydrogen bond interactions help the molecules to pack in an optimized manner so that there is addition of the individual dipole moments which in turn contributes to the NLO properties of the material. In FMBC, the molecular dipoles are stacked into layers along c-direction (Fig. 9) but with an angle inclination of 66.38^o between the adjacent dipoles (Fig. 10). Thus, though the molecules are nearly planar, the net dipole moment within a unit cell is quite small and hence observed β value of FMBC is less than some of the earlier reported materials (Table 5). Furthermore, optical excitation of the sample results in $\pi - \pi^*$ electronic transition within the aromatic part of the molecule, which has a longer lifetime in the excited states. These long lifetimes lead to the enhanced frequency of two photon resonance transitions which enhances the NLA via improved delocalization of π -electron and degree of π -conjugation [36]. Thus, the observed optical nonlinearity of FMBC can be attributed to its crystal structure consisting of planar molecules held in position by N-H \cdots O and C-H \cdots F hydrogen bond interaction.

The ratio σ_{ex}/σ_g is the figure of merit (FOM) for a material, the magnitude of which determines the optical limiting (OL) property. Optical limiting (OL) is the ability of a material to allow low-intensity radiation to pass through while blocking high-intensity radiation after a certain threshold. These types of devices are very useful in protecting human eyes, optical sensors, and such sensitive systems from intense laser beams. From Table 4, it is clear that FOM for FMBC is much greater than unity and thus we believe that it is a good material candidate for optical limiting devices for controlling CW laser intensities of μW to KW power. The OL behavior was extracted using the open aperture z scan experimental technique by plotting normalized transmittance against the input fluence and is shown in Fig. 19. In the case of an open aperture z scan experiment employing a Gaussian beam, the position-dependent fluence at point z along the beam was calculated using the equation,

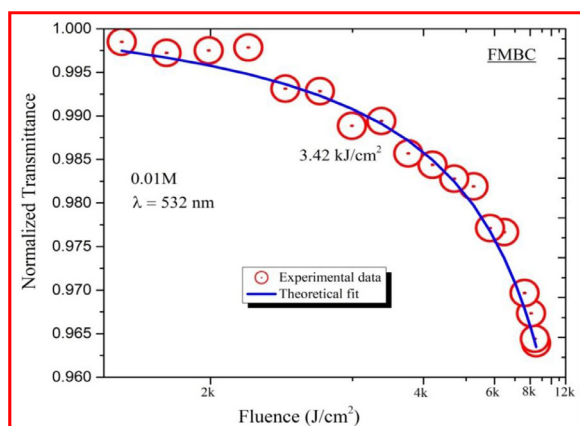
$$F(z) = 4(\ln 2)^{1/2} E_{in} / \pi^{3/2} w_0^2 [1 + (z/z_0)^2]^{-1/2} \quad (7)$$

where E_{in} is the input laser energy, w_0 is the beam waist at the focus and $z_0 = \pi w_0^2 / \lambda$ Rayleigh range. For lower intensity/fluence of the incident radiation, the transmittance exhibits almost linear behavior to the incident intensity (Fig. 19). As the input intensity increases beyond the threshold (3.42 kJ/cm²), the sample absorbs more light and hence limits the intensity of the transmitted beam. It is astonishing to note that FMBC has a better OL capacity compared to some of the previously reported materials (Table 5). Thermal defocusing, self diffraction and reverse saturable absorption (RSA) might cause optical limitation in a material. Since $\sigma_{ex} \gg \sigma_g$,

Table 5

Comparison of NLO parameters of FMBC with reported organic materials under similar experimental conditions.

n_2	β	χ^3	γ_h	OL Threshold	Melting Point
Compound (cm^2/W) (cm/W) (esu) (esu) $\times 10^{-8} \times 10^{-6} \times 10^{-7} \times 10^{-26} \times 10^3$	(J/cm^2)	($^\circ C$)			
[*]FMBC	-1.568	2.22 6.72 4.877 3.42	242.5		
[28]Br-ANC	-0.408		9.0	2.33	-
[29]3CAMC	-0.23		5.1	2.0	0.81 6.13 170.12
[25]DMAP4P	-4.21		4.1	2.41	- 5.32 160
[27]MFNP	-0.252		1.5	1.44	0.593 1.85 136
[30]NPTMP -0.437	7.8		-	-	6.75 145
[31]FMC	-0.1466		45	0.126	0.1044 11.2 -
[32]F3BC	-0.45		55	3.8	1.57 7.41 108.5
[32]F3NC	-1.31		12	11.3	4.64 1.92 177
[33]2ATN	-0.246		33.5	1.78	- 4.12 147.7

**Fig. 19.** Optical Limiting behavior of FMBC.

the condition for RSA, the observed OL property of FMBC is ascribed to RSA [37]. The one-photon FOM, $W = n_2 I / \alpha \lambda$ and two-photon FOM, $T = \beta \lambda / n_2$ for FMBC were calculated from n_2 and β values. For all-optical switching applications, W must be greater than unity and T must be less than unity [29]. In the present investigation, the determined values are satisfying this target condition and hence FMBC could be a potential material for optical switching applications.

4. Conclusion

A Schiff based hydrazone derivative, FMBC was synthesized and studied experimentally and theoretically, the results of which are reported in this article. The synthesized compound was established by FTIR spectral analysis. The TG/DTA thermal analysis shows that the material melts at 242.5 °C and decomposes at 359.5 °C. The optical transparency window of the material was obtained by UV-Vis spectroscopy and the optical band gap estimated by Tauc's plot is found to be equal to 3.44 eV. The blue light emission property of FMBC was investigated by photoluminescence spectral studies. The crystal structure is stabilized by N-H...O, C-H...O, and C-H...F hydrogen bond interactions. A deeper insight into various types of intermolecular interactions that contribute to the crystal packing was analyzed by HS analysis, 2D fingerprint plots, calculation of interaction energies, and the 3D energy frameworks using crystal explorer computer program. The estimated ER values show that C...H, N...H, O...H, and F...H are the favored contacts. The intermolecular energy calculations show that dispersive types of interactions are predominant over the crystal packing. The magnitudes of the third-order NLO parameters viz, the nonlinear absorption (β), the nonlinear refractive index (n_2),

and the nonlinear optical susceptibility ($\chi^{(3)}$) were estimated by single beam z scan experiment under CW regime and are found to be $2.22 \times 10^{-6} cm/W$, $-1.568 \times 10^{-8} cm^2/W$, and $6.72 \times 10^{-7} esu$ respectively. Furthermore, FMBC shows reverse saturable absorption as the condition of $\sigma_g < \sigma_{ex}$ was satisfied and thus capable of limiting the high power radiations with a limiting threshold of $3.24 kJ/cm^2$. The exceptional results make FMBC, a potential material for optical limiting and switching applications.

CRedit author statement: Author contributions

Laxminarayana Kamath: Conceptualization, Acquisition of data

Anthoni Praveen Menezes: Conceptualization, Methodology Analysis and/or interpretation of data, drafting the original manuscript

Raghavendra Bairy: Software, Validation, and Revision.

K. Shashi Kumar: Revising the manuscript

A. Jayarama: Supervision, revising the manuscript, and editing.

This statement is signed by (on behalf of all the authors)

Anthoni Praveen Menezes (signed on 21-10-2020)

Declaration of competing interest

The authors declare that they have no known competing financial interests or personal relationships that could have appeared to influence the work reported in this paper.

References

- [1] P.N. Prasad, Introduction to Nonlinear Optical Effects in Molecules and Polymers /Paras N. Prasad and David J. Williams., Wiley, New York, n.d.
- [2] S.R. Marder, C.B. Gorman, F. Meyers, J.W. Perry, G. Bourhill, J.L. Brédas, B.M. Pierce, A unified description of linear and nonlinear polarization in organic polymethine dyes, *Science* 265 (80-) (1994), doi:10.1126/science.265.5172.632.
- [3] S. Velmathi, V. Reena, Synthesis, characterization and investigation of the third order nonlinear optical properties of pyrrole Schiff bases, *Adv. Mater. Res.* (2012), doi:10.4028/www.scientific.net/AMR.488-489.377.
- [4] T.C. Wei, S. Mokkapat, T.Y. Li, C.H. Lin, G.R. Lin, C. Jagadish, J.H. He, Nonlinear Absorption Applications of CH₃NH₃PbBr₃ Perovskite Crystals, *Adv. Funct. Mater.* 28 (2018), doi:10.1002/adfm.201707175.
- [5] M. Saravanakumar, J. Chandrasekaran, M. Krishnakumar, B. Babu, G. Vinita, M. Anis, Experimental and quantum chemical studies on SHG, Z-scan and optical limiting investigation of 2-amino-5-bromopyridinium trifluoroacetate single crystal for optoelectronic applications, *J. Phys. Chem. Solids.* 136 (2020), doi:10.1016/j.jpcs.2019.109133.
- [6] Y. Takahashi, H. Adachi, T. Taniuchi, M. Takagi, Y. Hosokawa, S. Onzuka, S. Brahadewarar, M. Yoshimura, Y. Mori, H. Masuhara, T. Sasaki, H. Nakanishi, Organic nonlinear optical DAST crystals for electro-optic measurement and terahertz wave generation, *J. Photochem. Photobiol. A Chem.* 183 (2006), doi:10.1016/j.jphotochem.2006.03.027.
- [7] M. Rajkumar, A. Chandramohan, Synthesis, growth, structural, optical, thermal, electrical and mechanical properties of hydrogen bonded organic salt

- crystal: Triethylammonium-3, 5-dinitrosalicylate, *J. Mol. Struct.* 1134 (2017), doi:10.1016/j.molstruc.2017.01.034.
- [8] R. Brehme, D. Enders, R. Fernandez, J.M. Lassaletta, Aldehyde N,N-dialkylhydrazones as neutral acyl anion equivalents: umpolung of the imine reactivity, *Eur. J. Org. Chem.* (2007), doi:10.1002/ejoc.200700746.
- [9] H. Purandara, S. Raghavendra, S. Foro, P. Patil, B.T. Gowda, S.M. Dharmaprakash, P. Vishwanatha, Synthesis, spectroscopic characterization, crystal structure, Hirshfeld surface analysis and third-order nonlinear optical properties of 2-(4-chlorophenoxy)-N'-[(1E)-1-(4-methylphenyl) ethylidene] acetohydrazide, *J. Mol. Struct.* 1185 (2019), doi:10.1016/j.molstruc.2019.02.079.
- [10] S. Vijayakumar, A. Adhikari, B. Kalluraya, K.N. Sharafudeen, K. Chandrasekharan, Study of third-order optical nonlinearities of substituted hydrazones in PMMA, *J. Appl. Polym. Sci.* 119 (2011), doi:10.1002/app.32691.
- [11] G. Dutkiewicz, B. Narayana, S. Samsuddin, H.S. Yathirajan, M. Kubicki, Synthesis and crystal structures of two new Schiff base hydrazones derived from biphenyl-4-carbohydrazide, *J. Chem. Crystallogr.* 41 (2011), doi:10.1007/s10870-011-0118-3.
- [12] S. Turner, J. M., S.K. Mckinnon, Wolff, *CrystalExplorer17*, *Univ. West. Aust.* 63 (2017).
- [13] M. Sheik-Bahae, A.A. Said, T.H. Wei, D.J. Hagan, E.W. Van Stryland, Sensitive measurement of optical nonlinearities using a single beam, *IEEE J. Quantum Electron.* 26 (1990), doi:10.1109/3.53394.
- [14] A.P. Menezes, A. Jayarama, Role of direction of charge transfer on the nonlinear optical behavior of pyridine substituted chalcone derivatives, *J. Mol. Struct.* 1075 (2014), doi:10.1016/j.molstruc.2014.06.095.
- [15] S. Suresh, Studies on the optical and dielectric properties of a zinc thiourea chloride NLO single crystal, *Optik (Stuttg)* 125 (2014), doi:10.1016/j.ijleo.2013.07.154.
- [16] P.P. Vinaya, A.N. Prabhu, K. Subrahmanya Bhat, V. Upadhyaya, Synthesis, growth and characterization of a long-chain π -conjugation based methoxy chalcone derivative single crystal; a third order nonlinear optical material for optical limiting applications, *Opt. Mater. (Amst)*. 89 (2019), doi:10.1016/j.optmat.2019.01.061.
- [17] A. Priyadarshini, S. Kalainathan, Bulk crystal growth, spectral, optical, thermal, electrical and third-order NLO properties of benzylidene malononitrile derivative single crystal: a promising material for nonlinear optical device applications, *J. Mater. Sci. Mater. Electron.* 29 (2018), doi:10.1007/s10854-017-8196-4.
- [18] M.A. Spackman, D. Jayatilaka, Hirshfeld surface analysis, *CrystEngComm* 11 (2009) 19–32, doi:10.1039/B818330A.
- [19] S.L. Lee, A.L. Tan, D.J. Young, M.M. Jotani, E.R.T. Tiekink, 2Z)-3-Hydroxy-1-(pyridin-2-yl)-3-(pyridin-3-yl)prop-2-en-1-one: crystal structure and Hirshfeld surface analysis, *Acta Crystallogr. Sect. E Crystallogr. Commun.* 72 (2016), doi:10.1107/S205698901600832X.
- [20] S.L. Tan, M.M. Jotani, E.R.T. Tiekink, Utilizing Hirshfeld surface calculations, non-covalent interaction (NCI) plots and the calculation of interaction energies in the analysis of molecular packing, *Acta Crystallogr. Sect. E Crystallogr. Commun.* 75 (2019), doi:10.1107/S2056989019001129.
- [21] C. Jelsch, K. Ejsmont, L. Huder, The enrichment ratio of atomic contacts in crystals, an indicator derived from the Hirshfeld surface analysis, *IUCrj* 1 (2014), doi:10.1107/S2052252514003327.
- [22] C.F. Mackenzie, P.R. Spackman, D. Jayatilaka, M.A. Spackman, CrystalExplorer model energies and energy frameworks: extension to metal coordination compounds, organic salts, solvates and open-shell systems, *IUCrj* 4 (2017), doi:10.1107/S205225251700848X.
- [23] M.J. Turner, S. Grabowsky, D. Jayatilaka, M.A. Spackman, Accurate and efficient model energies for exploring intermolecular interactions in molecular crystals, *J. Phys. Chem. Lett.* 5 (2014), doi:10.1021/jz502271c.
- [24] Z.S.M.M.M. Fadhul, E.A.H.F. Ali, S.R. Maidur, P.S. Patil, M. Shkir, F.Z. Henari, Thermally induced optical nonlinearity and optical power limiting action of 2,4,5-trimethoxy-4'-nitrochalcone under CW laser regime, *J. Nonlinear Opt. Phys. Mater.* 27 (2018), doi:10.1142/S0218863518500121.
- [25] S. Raghavendra, T. Chandra Shekhara Shetty, C.S. Chidan Kumar, S. Naveen, S. Chandrāju, S.R. Maidur, P. Shankaragouda Patil, G.S. Ananthnag, S.M. Dharmaprakash, Novel acentric D- π -A- π -D nonlinear optical (2E, 4E)-[dimethylamino) phenyl]-1-(4methylphenyl)penta-2,4-dien-1-one crystal for second and third order nonlinear applications, *J. Chem. Sci.* 132 (2020), doi:10.1007/s12039-020-01764-7.
- [26] A.P. Menezes, S. Raghavendra, A. Jayarama, H.P. Sarveshwara, S.M. Dharmaprakash, Structural, thermal, linear and nonlinear optical studies of an organic optical limiter based on reverse saturable absorption, *J. Mol. Struct.* 1119 (2016), doi:10.1016/j.molstruc.2016.04.052.
- [27] S. Satheeshchandra, A.P. Menezes, H.P. Sarveshwara, A. Jayarama, The significant role of molecular dipole arrangements on the second and third-order nonlinear optical properties of a furan based chalcone, *Phys. B Condens. Matter.* 599 (2020), doi:10.1016/j.physb.2020.412501.
- [28] S.R. Maidur, J.R. Jahagirdar, P.S. Patil, T.S. Chia, C.K. Quah, Structural characterizations, Hirshfeld surface analyses, and third-order nonlinear optical properties of two novel chalcone derivatives, *Opt. Mater. (Amst)*. 75 (2018), doi:10.1016/j.optmat.2017.11.008.
- [29] A.P. Menezes, S. Raghavendra, T.S. Chia, C.K. Quah, Structure and nonlinear optical properties of (E)-1-(4-aminophenyl)-3-(3-chlorophenyl) prop-2-en-1-one: A promising new D- π -A- π -D type chalcone derivative crystal for nonlinear optical devices, *J. Mol. Struct.* 1129 (2017), doi:10.1016/j.molstruc.2016.09.077.
- [30] S.R. Prabhu, V. Parol, V. Upadhyaya, A. Jayarama, S.R. Maidur, P.S. Patil, Novel nitro based chalcone derivative single crystals: characterization on structural, linear optical, thermal, and third-order nonlinear optical properties, *Appl. Phys. A Mater. Sci. Process.* 126 (2020), doi:10.1007/s00339-020-04039-7.
- [31] A. Ekbote, S.R. Maidur, P. Shankaragouda Patil, Third-order NLO properties and power limiting behavior of (E)-3-(4-fluorophenyl)-1-(4-methoxyphenyl)prop-2-en-1-one under CW laser excitation, *Mater. Today Proc* (2020), doi:10.1016/j.matpr.2020.02.054.
- [32] A. Ekbote, P.S. Patil, S.R. Maidur, T.S. Chia, C.K. Quah, Structural, third-order optical nonlinearities and figures of merit of (E)-1-(3-substituted phenyl)-3-(4-fluorophenyl) prop-2-en-1-one under CW regime: New chalcone derivatives for optical limiting applications, *Dye. Pigment.* 139 (2017), doi:10.1016/j.dyepig.2017.01.002.
- [33] H. Davanagere, J. Arasali, C.K. Quah, H.C. Kwong, P.S. Patil, Investigation of structural, physical, linear, and nonlinear optical properties of two novel thiophene centred D- π -A type push-pull organic derivatives for nonlinear optical applications, *J. Mol. Struct.* 1220 (2020), doi:10.1016/j.molstruc.2020.128763.
- [34] A. Jayarama, H.J. Ravindra, A.P. Menezes, S.M. Dharmaprakash, S.W. Ng, Synthesis, growth, and characterization of 3-(4-Methoxyphenyl)-1-(pyridin-2-yl) prop-2-en-1-one single crystal: A potential NLO material, *J. Mol. Struct.* 1051 (2013), doi:10.1016/j.molstruc.2013.08.026.
- [35] D. Fichou, T. Watanabe, T. Takeda, S. Miyata, Y. Goto, M. Nakayama, Influence of the ring-substitution on the second harmonic generation of chalcone derivatives, *Jpn. J. Appl. Phys.* 27 (1988), doi:10.1143/JJAP.27.L429.
- [36] S. Anandan, S. Manoharan, N.K.S. Narendran, T.C.S. Girisun, A.M. Asiri, Donor-acceptor substituted thiophene dyes for enhanced nonlinear optical limiting, *Opt. Mater. (Amst)*. 85 (2018), doi:10.1016/j.optmat.2018.08.004.
- [37] V.S. Naik, P.S. Patil, Q.A. Wong, C.K. Quah, N.B. Gummagol, H.S. Jayanna, Molecular structure, linear optical, second and third-order nonlinear optical properties of two non-centrosymmetric thiophene-chalcone derivatives, *J. Mol. Struct.* (2020) 1222, doi:10.1016/j.molstruc.2020.128901.